Optimizing the Sequence of Combination Therapy with Radiolabeled Antibodies and Fractionated External Beam

Shutian Ruan, Joseph A. O'Donoghue, Steven M. Larson, Ronald D. Finn, Achim Jungbluth, Sydney Welt, and John L. Humm

Department of Medical Physics and Nuclear Medicine, Department of Radiology, and The Ludwig Institute for Cancer Research, Memorial Sloan-Kettering Cancer Center, New York, New York

The purpose of this study was to determine the optimum sequence for combined modality therapy with radiolabeled antibodies and fractionated external beam radiation. **Methods:** The uptake and distribution of a nontherapeutic activity of ^{125}I-labeled tumor-associated A33 monoclonal antibody was determined in SW1222 human colon carcinoma xenografts in nude mice for 4 study groups: group 1, radiolabeled antibody alone; group 2, radiolabeled antibody administered (day 0) immediately before the first of 5 daily fractions of 2-Gy, 320-kilovolt peak x-rays; group 3, radiolabeled antibody administered after the fifth radiation fraction (day 5); and group 4, radiolabeled antibody administered 5 d after irradiation (day 10). Tumors were excised 5 d after antibody administration. Tumors were frozen and sectioned for histology and phosphor plate autoradiography. The percentage of A33 antigen-expressing cells was estimated by immunohistochemical staining. **Results:** The average tumor uptake values relative to control group 1 were 1.47 (group 2), 0.78 (group 3), and 0.21 (group 4), which illustrates that tumor uptake is increased by almost 50% when the antibody is present in the blood at the start of irradiation. Five days into a fractionated irradiation protocol, antibody uptake was reduced, falling more significantly on day 10. Phosphor plate autoradiographs showed decreased uptake uniformity for groups 3 and 4. Immunohistochemical data showed a reduction in A33 antigen-positive cells from 85%, 64%, 50%, to 41% for groups 1–4, respectively. **Conclusion:** Maximum radiolabeled antibody tumor uptake was achieved when the antibody was administered just before radiation therapy. This might be explained by a transient increase in capillary leakage to macromolecules, followed by a reduction at later times, possibly the result of capillary damage and occlusion.

Key Words: radioimmunotherapy; radiation therapy; A33 antibody; immunohistochemistry; phosphor plate autoradiography

J Nucl Med 2000; 41:1905–1912

Radioimmunotherapy (RIT) is a promising, yet controversial, treatment modality. Numerous clinical RIT trials have been performed with antibodies directed against refractory bulk disease of different types of cancers: ovarian (*1*), prostate (*2*), colon (*3*), renal (*4*), neurologic (*5*), lymphoma (*6*), and so forth. The trials have shown few durable responses in bulk tumors, with the exception of patients with small-volume disease (*1*), highly radiosensitive lymphomas (*6*), or disseminated malignancies in the cerebral spinal fluid (*7*). The radiation doses delivered to tumors by RIT (range, 15–50 Gy) are unlikely to be tumoricidal to bulk disease if RIT is used as the sole treatment modality.

In contrast, advances in external beam radiotherapy (XRT) have resulted in progressive dose escalation to prostate, breast, lung, and brain tumors. For example, radiation doses to prostate tumors have been increased from 65 to 81 Gy through the introduction of CT planning and conformal techniques (*8*) and to 86.4 Gy and beyond by the use of intensity modulation (*9*). This dose escalation is designed to improve local control and, thereby, it is hypothesized, also to reduce or delay metastatic spread. However, treatment failures still occur within and at the periphery of the high-dose volume as well as associated with local and distant metastatic dissemination (*10*).

Combination therapy between RIT with chemotherapy has been proposed as a means to boost treatment efficacy (*11–13*). However, there is no current basis for combining the cytotoxicities of these 2 modalities. One advantage of combining RIT with XRT is the possibility of relating the cytocidal effects of both treatments to the physical parameter of absorbed dose. However, this assumes that 1 Gy of radiation dose delivered by radiolabeled antibodies is equivalent to 1 Gy delivered by conventional XRT.

There are 3 major reasons why the simple addition of doses by the 2 modalities, to obtain a cumulative dose, may not be applicable. (a) The dose rate of XRT is 2 Gy per daily fraction, delivered as an acute irradiation exposure over 6–8 wk. This is compared with the delivery of 20–30 Gy by RIT within 1–2 wk, but at a continuous low-dose rate, typically from 0.3 Gy/h at an exponentially declining rate. (b) The variation of dose within the target volume is small for XRT (by design, $<$10%), whereas in RIT it may vary dramatically (dependent on the targeting molecule). (c) There may be

Received Oct. 29, 1999; revision accepted May 5, 2000.

For correspondence or reprints contact: John L. Humm, PhD, Department of Medical Physics, Memorial Sloan-Kettering Cancer Center, 1275 York Ave., New York, NY 10021.

some immunotoxicity associated with the antibody binding (*6,14*). As a consequence of such obstacles, the interpretation of combination RIT with XRT will be difficult.

Several studies have been performed to compare the effectiveness of RIT with XRT in experimental animal model systems. Langmuir et al. (*15*) reviewed 5 studies comparing the effects of RIT with single-dose or fractionated XRT on xenografted tumors. Biologic enhancement factors were defined as the ratio of absorbed doses from XRT to RIT to give the same level of response. These ranged from 0.3 to 3.0 depending on the characteristics of the cell line and the details of the irradiation procedures. Roberson and Buchsbaum (*16*) compared RIT with single-fraction XRT in colon cancer xenografts. This resulted in an apparent relative efficacy factor of 0.3. However, by individually accounting for all radiobiologic and dosimetric features of the system, they found that the differences in biologic effects between modalities could be substantially reconciled. The most significant mechanism was heterogeneity in the RIT dose distribution.

Buchegger et al. (*17*) examined the use of combined XRT and RIT in an animal model system. A radiotherapy schedule consisting of 5 daily fractions was used in combination with RIT for treatment of colorectal cancer xenografts. The therapeutic effects of the combination were additive, but the toxicity of the combination was similar to that of RIT alone. In a resistant tumor that was impossible to control locally with the maximum achievable XRT, combined treatment gave 100% local control. More recently, the same group has reported that combined RIT and XRT was more effective than either modality alone in the treatment of liver metastases from colorectal cancer in an animal model system (*18*). The time scheduling of combined modality therapy also appears to be a significant factor with concurrent administrations apparently more efficacious than sequential administration (*19*). In terms of sequential administrations, little difference in growth delay was found between XRT followed by RIT and RIT followed by XRT. However, tumor regression was more pronounced after XRT followed by RIT. These studies were purely phenomenological; differences in antibody distribution consequent on external beam irradiation were not examined.

Various biologic mechanisms influence antibody uptake in tumors. Elevated interstitial fluid pressure (*20*) within tumors acts to reduce or eliminate the bioavailability of therapeutic molecules and becomes progressively more severe from peripheral to central regions. The existence of a binding site barrier (*21*) may also restrict antibody penetration into tumors because of binding at the first encounter. This would lead to regions of high uptake near the surface of avascular micrometastases (*22*) or in the vicinity of capillary vessels coupled with low uptake in more distant regions. Whereas radiolabeled antibody uptake and average tumor dose are important in the determination of tumor response, the effectiveness of the dose will depend on the specific radiolabel distribution within the tumor. It will depend, in particular, on the degree of uniformity in the association of the radiolabeled antibody with tumor cells (*23,24*).

The rationale for combining RIT with XRT is summarized as follows:

- RIT will boost the dose to the primary disease site, with minimal expected overlapping toxicity with XRT.
- RIT could contribute a radiation dose to tumor cells, which may extend beyond the high-dose cone down the radiation field.
- RIT may selectively target known or occult metastatic disease sites outside of the radiation treatment portals.
- XRT may improve both the uptake and the uniformity of the radiolabeled antibody delivery to the tumor.

However, one question arises before considering combination RIT with XRT. Which is the most effective sequence for treatment? Should XRT be administered before RIT? The rationale for this strategy would be that XRT debulks (like surgery) the tumor, allowing a higher percentage uptake per gram of tumor (*25*). In addition, preirradiation may increase the permeability of the tumor capillary vasculature and improve antibody uptake (*26*).

However, the duration of clinical XRT is 6–8 wk, during which time metastatic growth and spread outside the irradiated volume would be largely unchecked. It is likely that the growth of subclinical microscopic disease would be especially rapid (*27*). This would favor the strategy of delivering the RIT at the earliest possible stage.

The focus of this study was to determine the delivery sequence of RIT relative to XRT, which would maximize the radiolabeled uptake and, consequently, radiation dose to the primary tumor.

MATERIALS AND METHODS

Animal Model

Twenty athymic nude mice (BALB/cAnN; National Cancer Institute, Frederick, MD) were injected subcutaneously in the right hind limb with 2×10^6 SW1222 cells (Ludwig Institute for Cancer Research, New York, NY). SW1222 is a colorectal carcinoma cell line of human origin, which expresses about 8×10^5 antigen binding sites per cell to the A33 antibody used in this study (*28*). After 10–12 d, the tumors reached an average size of 400–600 mg.

Antibody

The A33 antibody is a murine monoclonal IgG2a, which is internalized by antigen-positive cells through cytoplasmic vesicles, transported to perinuclear regions, and subsequently exteriorized in an intact form, thus enabling the process of uptake to repeat (*14*). The A33 antigen, defined by A33 monoclonal antibody, is a 43-kDa transmembrane glycoprotein in normal human colonic epithelium and endothelium (*29*). It is expressed on >95% of human colon cancers (*14*). In this study, a purified humanized A33 antibody was used. It was labeled with ^{125}I by the IODO-GEN (Pierce, Rockford, IL) method. Specific activities ranged from 177.6 to 185 MBq/mg antibody.

External Beam Irradiation

Mice were irradiated on a 320-kilovolt peak (kV_p) x-ray irradiator. Five mice per group were anesthetized with 0.5 mL 97% 2,2,2-tribromoethanol (Avertin; Pfaltz and Bauer, Waterbury, CT) by intraperitoneal injection and arranged around the edges of a 20×20 cm^2 radiation field. The tumor-bearing leg of each animal was extended and taped within the radiation or light field. The rest of the body remained outside of the primary field (to spare the normal body organs). The mice were irradiated for 5 consecutive days at 2 Gy per fraction, yielding a total dose of 10 Gy. The radiation beam was filtered by 2 mm of copper and delivered at a dose rate of 150 cGy/min at 50-cm source skin distance. The x-ray unit was calibrated using a Holt ionization chamber of 0.06-mL volume, 8-mm outer diameter, with a 1-mm buildup cap. Field flatness was within ±3% as confirmed by Kodak V film (Eastman Kodak, Rochester, NY).

Histology

The excised tumors from 4 of 5 mice, for each group, were embedded in OCT (Miles Inc., Elkhart, IN) and frozen on dry ice in a cryomold. The blocks were cut on a cryostat microtome (Brightman, Chelmsford, UK) in 8-μm sections. Sections were fixed in 10% phosphate-buffered formalin for 5 min, washed twice, and then dried. Sections were stained with hematoxylin and eosin (H and E) or used for autoradiography. One tumor specimen per group was fixed in 10% buffered formalin and then processed for paraffin embedding. Five-micron tissue sections were cut and stained with H and E to examine tumor morphology.

Immunochemistry

Expression of the A33 antigen was examined in the tumor xenografts using the Vectastain avidin-biotinylated peroxidase staining system (Vector Laboratories, Burlingame, CA). Briefly, frozen sections were fixed in cold acetone for 10 min, followed by washing 3 times with phosphate-buffered saline (PBS). The sections were incubated for 30 min with 1% fatty acid–free bovine serum albumin (BSA-PBS; Calbiochem, San Diego, CA) for blocking nonspecific binding and then transferred into 0.3% hydrogen peroxide PBS for 15 min to quench the endogenous peroxidase activity. After a further rinse, the sections were incubated with humanized A33 antibody (10 μg/mL in BSA-PBS) for 60 min. The biotinylated secondary rabbit antihuman antibody was then added, followed by avidin-biotinylated peroxidase complex reagents. The staining was developed with the substrate diaminobenzidine tetrahydrochloride according to the manufacturer's instructions. Finally, tumor sections were counterstained with hematoxylin to display tumor morphology together with cell-associated A33 antigen expression.

Autoradiography

The tissue sections from all 4 study groups were mounted on a piece of card and then pressed simultaneously in contact with a phosphor storage screen (type BI). The screen was exposed for a duration of 7 d within a light-tight cassette. The screen was read out on a GS-363 Molecular Imager (BioRad, Hercules, CA) laser scanner at the highest spatial resolution of 100×100 μm (*30*,*31*).

Study Design

Humanized ^{125}I-labeled IgG2a A33 antibody (1.036 MBq/8 μg) was injected intravenously into the mice before, simultaneously with, or after XRT. Four groups of 5 animals (20 mice in total) were studied. In each study group, 1 of the 5 animals was not injected with the radiolabel but was handled in every other regard in a way that was identical with the handling of the remainder of the group. This was done to observe the effects of external beam radiation on the tumor tissue at different times after treatment with high-quality paraffin sections. The experimental design is summarized in Figure 1. Animal tumors were selected to be of the same size range, 0.4–0.6 g, at the initiation of XRT for all study groups.

In group 1, 4 of the 5 animals were injected with a diagnostic dose (1.85 MBq) of ^{125}I-labeled humanized A33 antibody. No XRT followed. This group was used to study the antibody uptake and microdistribution of radiolabeled antibody alone, which is operationally identical to the case of a course of RIT preceding XRT—that is, when the radiolabeled antibody uptake has already peaked. All 5 animals were killed on day 5, and the tumors were excised and counted on a γ counter (Wallac, Turku, Finland) with a window setting for 25- to 35-keV photons. After counting, the tumors were embedded in OCT, frozen, and sectioned for autoradiography. In the fifth animal, the tumor was fixed in 10% formalin and prepared for paraffin embedding, sectioning, and staining.

In group 2, 4 of the 5 animals were injected with 1.85 MBq ^{125}I-labeled humanized A33 antibody. All 5 animals were then administered the first 2-Gy fraction of 320-kV_p x-rays; daily fractions of x-rays were administered thereafter. On day 5, 6 h after administration of the fifth fraction, all animals were killed. Tumors were excised, counted, frozen, and sectioned for autoradiography. The nonradioactive tissue specimen was fixed in formalin and embedded in paraffin. This tissue was used to assess the effect of radiation damage 5 d after XRT.

In group 3, the tumors were first irradiated with 5 fractions of external beam x-rays. On day 5, 4 of the 5 animals were injected

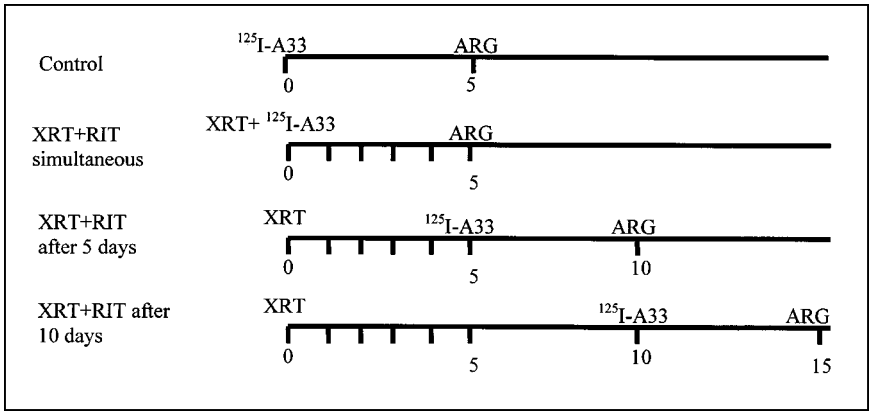

FIGURE 1. Schematic diagram of 4 study groups. ARG = autoradiography.

with 1.85 MBq ^{125}I-labeled humanized A33 antibody. On day 10, all animals were killed, and the tumors were processed as described. The nonradioactive tissue specimen was fixed in formalin and embedded in paraffin, and this tissue was used to assess the effect of radiation damage 10 d after XRT.

In group 4, the tumors were irradiated with 5 daily fractions. Then a 5-d break ensued before the radiolabeled antibody was injected into 4 of the 5 mice on day 10. All mice were killed on day 15, and the tumors were processed as for the other groups.

The principal objective of the study design was to investigate the effect of pretumor irradiation on antibody uptake and microdistribution. For this reason, all animals were given the same diagnostic activity (1.85 MBq) of ^{125}I-labeled antibody, resulting in negligible radiation damage from the radiolabeled antibody. All animals were killed 5 d after administration of the radiolabeled antibody to allow equal time for antibody uptake and redistribution (Fig. 1).

RESULTS

Changes in Tumor Histology and Antigen Expression

Figure 2 illustrates the tumor morphology for the 4 groups. Figures 2A–D, corresponding to study groups 1–4, show the progression of histologic changes with time after irradiation. Figure 2A shows an example field of the nonirradiated control SW1222 tumor (group 1). It reveals an adenocarcinoma without morphological signs of regression or necrosis. Figure 2B shows the changes on day 5, after a course of 5 daily fractions of 2 Gy (group 2). The glandular structure is only partially preserved. The tumor cells are less coherent, and necrotic cells and debris are visible. The interstitial spaces are widened and indicate edematous changes. Figure 2C shows the tumor histology on day

COLOR

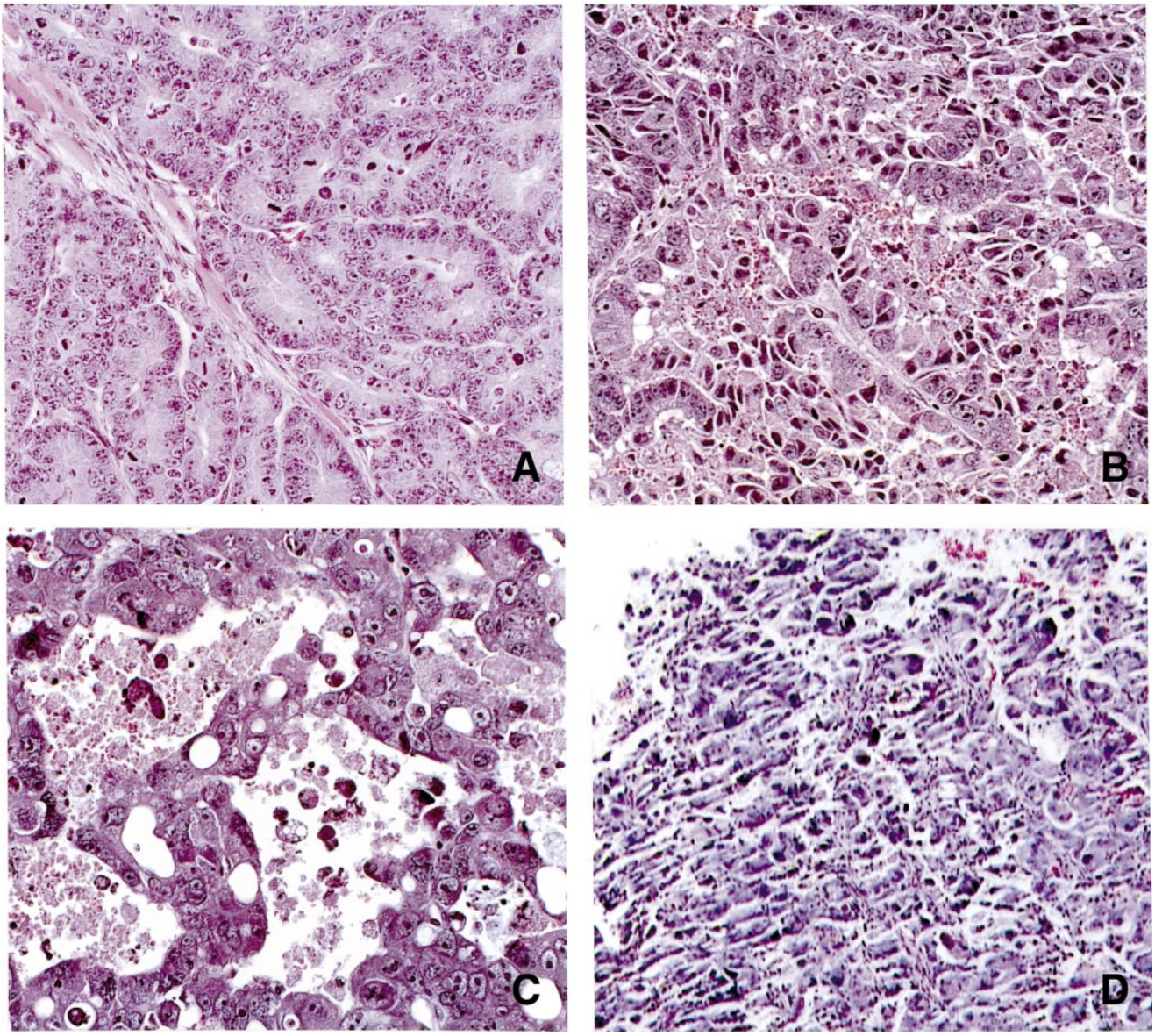

FIGURE 2. H- and E-stained sections from paraffin blocks show changes in tumor histology for groups 1–4. Radiation was delivered in 5 2-Gy fractions on days 0–4. (A) Group 1 (control), ×100 magnification. (B) Group 2 (day 5 after initiation of radiation therapy), ×100 magnification. (C) Group 3 (day 10 after initiation of radiation therapy), ×200 magnification. (D) Group 4 (day 15 after initiation of radiation therapy), ×100 magnification.

10—that is, 5 d after the completion of XRT (group 3). At this time, the glandular structure has completely disappeared. The cell density has dropped, and there are pools of edema. In Figure 2D (group 4), large regions of the tumor have become necrotic, and there is widespread breakdown of the structural integrity of the tissue.

Figure 3 is composed of 4 photographs that correspond to groups 1–4. These are frozen tumor sections that have been stained for A33 antigen expression. The control (Fig. 3A) shows uniform immunoperoxidase staining, which covers the entire section. In Figure 3B, shown at higher magnification, there appears to be a slight reduction in the fraction of A33 antigen-positive cells. However, the staining is still restricted to the cell surface membrane. For group 3 (Fig. 3C), the antigen staining appears to be associated with not only the cellular membrane but also the intracellular domains. This is possibly a consequence of cellular radiation damage, breakdown, and necrosis. Finally, on day 15 (Fig. 3D), there are clustered regions of intense antigen expression, no longer exclusively cell associated, and enlarged areas with no antigen staining.

The cell density of 3 tumor frozen sections (stained with H and E) of each study group was measured by counting of number of cells within the squares of an eyepiece graticule. Values for the average number of cells per square millimeter are given in Table 1. Furthermore, the fraction of cells staining positive for the A33 antigen was also determined (Table 1).

These results show, first, that the cell density within the tumor gradually decreases with time after irradiation, falling

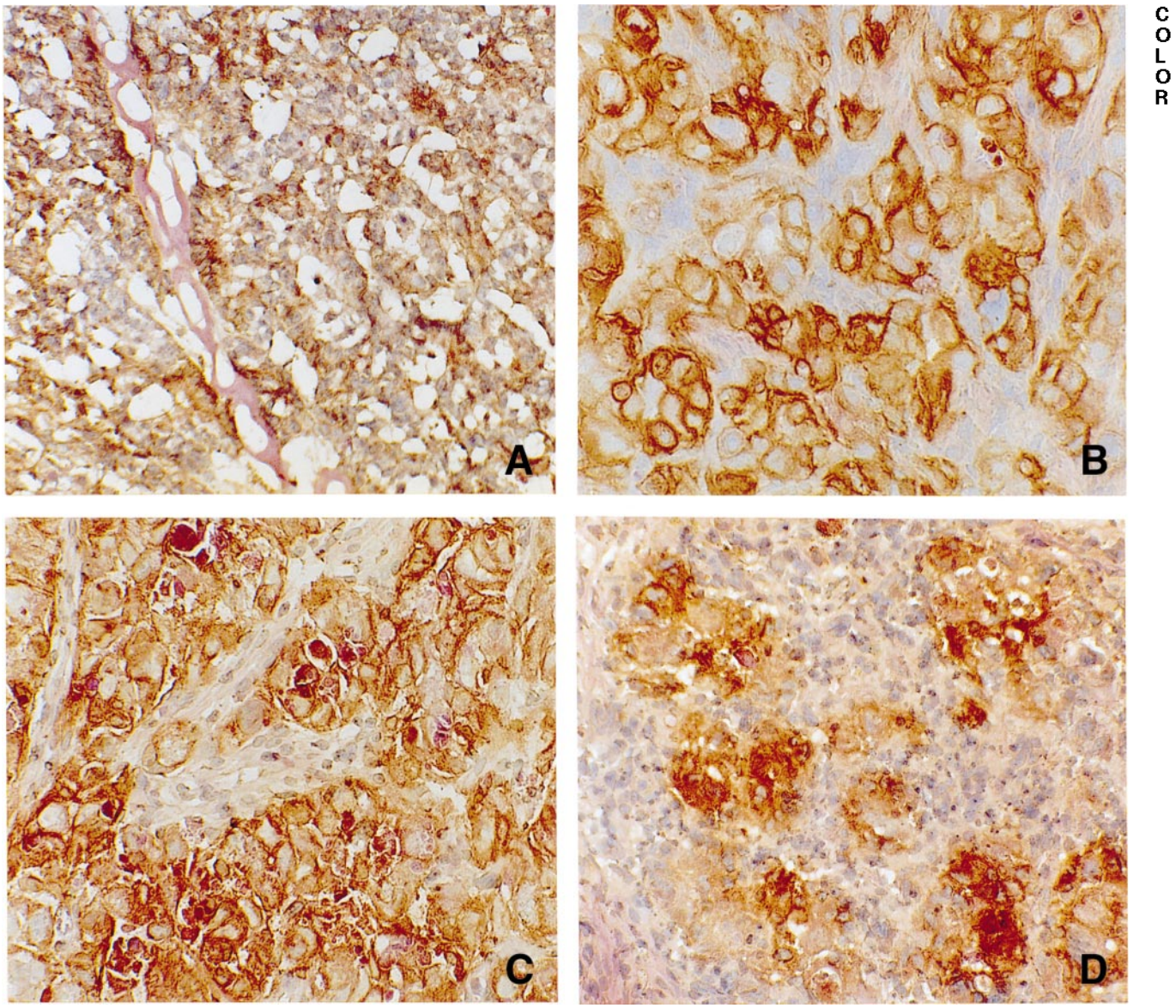

COLOR

FIGURE 3. Immunoperoxidase- and H- and E-stained frozen sections show changes in tumor histology for groups 1–4. (A) Group 1 (control), ×100 magnification. (B) Group 2 (day 5 after initiation of radiation therapy), ×200 magnification. (C) Group 3 (day 10 after initiation of radiation therapy), ×100 magnification. (D) Group 4 (day 15 after initiation of radiation therapy), ×100 magnification.

TABLE 1
Measurements of Cell Number and Fraction That Stained Positive for A33 Antigen on Frozen Tissue Sections for 4 Study Groups

Group	Cell no./mm^2	% Antigen positive
1 (day 0, no XRT)	5550	85.2
2 (day 5, XRT days 1–5)	4115	64.4
3 (day 10, XRT days 1–5)	3190	50.4
4 (day 15, XRT days 1–5)	2910	41.3

to almost 50% 15 d after the initiation of XRT. This is a consequence of cell loss and the expansion of tissue edema. Second, the fraction of the residual cells expressing antigen also slowly diminishes with time after irradiation. This is a consequence of a reduction in the ratio of tumor cells to normal stromal and inflammatory cells within the section. It may also be the consequence of a progressive loss of antigen expression by the doomed tumor cell population.

Changes in Radiolabeled Antibody Uptake and Distribution

The excised tumors of 4 animals per group were weighed and counted on a γ counter to determine the antibody uptake as percentage injected dose per gram (%ID/g) of tumor. Table 2 summarizes the average %ID/g ± SD for each of the 4 groups. For the nonirradiated control animals (group 1), the average %ID/g was 10.3, which is in agreement with previous studies performed by Barendswaard et al. (*32*). In group 2, where the animals were irradiated with the first 2-Gy fraction 30 min after administration of the radiolabeled antibody, there was an average increase of 50% in tumor uptake. However, when the radiolabeled antibody was administered at the end of 5 fractions of XRT (group 3), the uptake returned to baseline. When the radiolabeled antibody was administered on day 10 (group 4), the %ID/g in the tumor was reduced to less than one fifth of the baseline values. These data are consistent with the histopathologic description of radiation damage by Casarett (*33*), who reported an initial transient increase in the leakiness of the capillaries after irradiation, followed by inflammation and thrombosis. In our study, the progressive deterioration and collapse of the normal stromal tissue elements, coupled with both cell and antigen loss, support this hypothesis.

Figure 4 shows a series of 8 phosphor plate autoradiographic images from the tumors. A representative section is shown for 2 of the tumors in each study group. The greatest uniformity of radiolabel is observed in the nonirradiated tumors (group 1). Group 2 exhibited, on average, a 50% higher radiolabeled antibody uptake. However, this did not translate, for any of the 4 tumors, into improved uniformity of the radiolabeled antibody distribution. Tumor irradiation, with the radiolabeled antibody present in the bloodstream, probably resulted in a more rapid extravasation of the antibody, with pooling into the already well-perfused regions of the tumor. For group 3, the tumors had already shrunk to about one half the diameter of the control at the time of animal killing. Although the tumor counts were greatly reduced relative to that of the nonirradiated animals, the %ID/g was not significantly lower than that of the nonirradiated control tumors (group 1) because of the compensatory reduction in tumor mass on day 10. The distribution of radiolabel within these sections exhibited a reduced uniformity. This trend increased in group 4 on day 15 after the start of XRT, when the tumors had shrunk to an even smaller size (< 0.15 g), and the %ID/g fell about 5-fold below that of the nonirradiated tumors of group 1.

TABLE 2
Measurements of Tumor Uptake in %ID/g Tumor ± SD for 4 Tumors per Group

Group	%ID/g tumor ± SD
1 (day 0, no XRT)	10.3 ± 6.1
2 (day 5, XRT days 1–5)	15.1 ± 6.3
3 (day 10, XRT days 1–5)	9.2 ± 7.5
4 (day 15, XRT days 1–5)	2.2 ± 0.3

DISCUSSION

To optimize a combined treatment approach, our understanding of the complex radiobiology of RIT needs to be improved. One important aspect is how to achieve the maximum therapeutic effect from radionuclide targeting at administered levels of activity within dose-limiting toxicity. Dose escalation is postulated to improve uptake of radiolabel in the tumor (*34*). However, without improvements in the microdistribution of activity within the tumor, this may not translate into an increase in the therapeutic response (*24*).

A systematic study of how the uptake and distribution of radiolabeled antibodies, with therapeutic potential, are perturbed by preirradiation of the tumor is necessary to provide a rational basis for the optimization of combined modality therapy. Many disease sites could benefit by the inclusion of RIT into the radiation therapy protocol. One example is rectal carcinoma. Here, the standard treatment for unresectable locally advanced disease is preoperative radiation therapy followed by surgery (*35*). The goal of preirradiation is to convert the status of the cancer to a resectable one. Normal tissue tolerance in the pelvis restricts the doses that can be delivered by XRT alone. Attempts to further improve local control by the addition of intraoperative electron irradiation have been explored. Local failure rates with preoperative XRT and intraoperative XRT have been reported to be 37% for primary disease (*36*). The addition of RIT to such a protocol may have significant promise, especially because any overlapping toxicity is unlikely.

We expect that combined therapy with RIT and XRT will capitalize on the strengths and address the weaknesses of both modalities. The study presented in this article focused on 1 aspect of combined RIT and XRT—namely, determination of the optimum delivery sequence of the 2 treatments. The therapeutic efficacy of the combined modality treatment was not addressed but, rather, we focused on the effects of

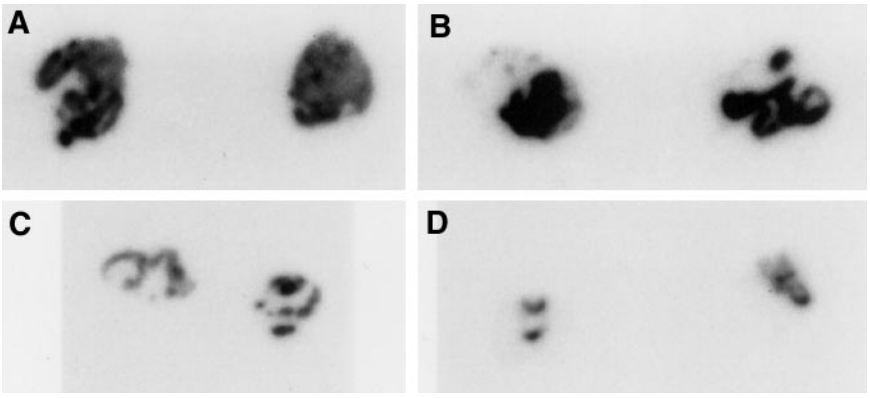

FIGURE 4. Digital phosphor plate autoradiographs from frozen tissue sections. Two sections (from 2 different tumors) for each study group (A, group 1; B, group 2; C, group 3; D, group 4) illustrate changes in antibody distribution. (A–D) Same magnification.

XRT on radiolabeled antibody uptake and distribution as a consequence of histopathologic changes.

CONCLUSION

The findings of this study suggest that tumor uptake is maximal when fractionated XRT is initiated immediately after injection of the radioimmunoconjugate because of a transient increase in the leakiness of the capillaries. In clinical practice, this would pose the logistic problem of the daily transport of radioactive patients into a radiation therapy suite. Nevertheless, the short daily exposure of the radiation therapists to the patient, relative to nuclear medicine technologists, does not suggest a serious increase in exposure burden to such personnel. In spite of our initial expectations, that pre-XRT would debulk the tumor, and thereby increase the %ID/g of the radiolabeled antibody, the opposite was found. Preirradiation of the tumor resulted in rapid structural degradation of the tumor stroma and vasculature, reducing tumor antibody uptake. Furthermore, we found that the amount of antigen expression decreased with the further effect of diminishing antibody–tumor targeting.

ACKNOWLEDGMENTS

This work was supported by grants from the National Cancer Institute (NCI 1R01 CA75412) and the Department of Energy (DE-FG02–86ER60407).

REFERENCES

1. Hird V, Maraveyas A, Snook D, et al. Adjuvant therapy of ovarian cancer with radioactive monoclonal antibody. *Br J Cancer*. 1993;68:403–406.
2. Meredith RF, Bueschen AJ, Khazaeli MB, et al. Treatment of metastatic prostate carcinoma with radiolabeled antibody CC49. *J Nucl Med*. 1994;35:1017–1022.
3. Begent RHJ, Ledermann JA, Green AJ, et al. Antibody distribution and dosimetry in patients receiving radiolabelled antibody therapy for colorectal cancer. *Br J Cancer*. 1989;60:406–412.
4. Divgi CR, Bander NH, Scott AM, et al. Phase I/II radioimmunotherapy trial with iodine-131-labeled monoclonal antibody G250 in metastatic renal cell carcinoma. *Clin Cancer Res*. 1998;4:2729–2739.
5. Kemshead JT, Hopkins K, Pizer B, et al. Dose escalation with repeated intrathecal injections of ^{131}I-labelled mAbs for the treatment of central nervous system malignancies. *Br J Cancer*. 1998;77:2324–2330.
6. Kaminski MS, Zasadny KR, Francis IR, et al. Iodine-131-anti-B1 radioimmunotherapy for B-cell lymphoma. *J Clin Oncol*. 1996;14:1974–1981.
7. Coakham HB, Kemshead JT. Treatment of neoplastic meningitis by targeted radiation using (131)I-radiolabelled monoclonal antibodies: results of responses and long term follow-up in 40 patients. *J Neurooncol*. 1998;38:225–232.
8. Leibel SA, Zelefsky MJ, Kutcher GJ, et al. The biological basis and clinical application of three-dimensional conformal external beam radiation therapy in carcinoma of the prostate. *Semin Radiat Oncol*. 1994;21:580–597.
9. Zelefsky MJ, Leibel SA, Kutcher GJ, et al. Three-dimensional conformal radiotherapy and dose escalation: where do we stand? *Semin Radiat Oncol*. 1998;8:107–114.
10. Gaudin PB, Zelefsky MJ, Leibel SA, et al. Histopathologic effects of three-dimensional conformal external beam radiation therapy on benign and malignant prostate tissues. *Am J Surg Pathol*. 1999;23:1021–1031.
11. Sitzmann JV, Abrams R. Improved survival for hepatocellular cancer with combination surgery and multimodality treatment. *Ann Surg*. 1993;217:149–154.
12. Cheung NK, Cheung IY, Canete A, et al. Antibody response to murine anti-GD2 monoclonal antibodies: correlation with patient survival. *Cancer Res*. 1994;54: 2228–2233.
13. DeNardo SJ, Kukis DL, Kroger LA, et al. Synergy of taxol and radioimmunotherapy with yttrium-90-labeled chimeric L6 antibody: efficacy and toxicity in breast cancer xenografts. *Proc Natl Acad Sci USA*. 1997;94:4000–4004.
14. Welt S, Scott AM, Divgi CR, et al. Phase I/II study of iodine-125 labeled monoclonal antibody A33 in patients with advanced colon cancer. *J Clin Oncol*. 1996;14:1787–1797.
15. Langmuir VK, Fowler JF, Knox SJ, et al. Radiobiology of radiolabeled antibody therapy as applied to tumor dosimetry. *Med Phys*. 1993;20:601–610.
16. Roberson PL, Buchsbaum DJ. Reconciliation of tumor dose response to external beam radiotherapy versus radioimmunotherapy with ^{131}iodine-labeled antibody for a colon cancer model. *Cancer Res*. 1995;55(suppl 23):5811S–5816S.
17. Buchegger F, Rojas A, Delaloye AB, et al. Combined radioimmunotherapy and radiotherapy of human colon carcinoma grafted in nude mice. *Cancer Res*. 1995;55:83–89.
18. Vogel CA, Galmiche MC, Buchegger F. Radioimmunotherapy of human colon cancer liver metastases in nude mice. *Cancer Res*. 1997;57:447–453.
19. Sun LQ, Vogel CA, Mirimanoff RO, et al. Timing effects of combined radioimmunotherapy and radiotherapy on a human solid tumor in nude mice. *Cancer Res*. 1997;57:1312–1319.
20. Jain RK. Delivery of novel therapeutic agents in tumors: physiological barriers and strategies. *J Natl Cancer Inst*. 1989;81:1–7.
21. Juweid M, Neumann R, Paik C, et al. Micropharmacology of monoclonal antibodies in solid tumors: direct experimental evidence for a binding site barrier. *Cancer Res*. 1992;52:5144–5153.
22. Saga T, Neumann RD, Heya T, et al. Targeting cancer micrometastases with monoclonal antibodies: a binding-site barrier. *Proc Natl Acad Sci USA*. 1995;92: 8999–9003.
23. Humm JL, Chin LM, Cobb LM, et al. Microdosimetry in radioimmunotherapy. *Radiat Prot Dosim*. 1990;31:433–436.
24. O'Donoghue JA. Implications of nonuniform tumor doses for radioimmunotherapy. *J Nucl Med*. 1999;40:1337–1341.
25. Pedley RB, Boden J, Keep PA, et al. Relationship between tumour size and uptake of radiolabelled anti-CEA in a colon tumour xenograft. *Eur J Nucl Med*. 1987;13:197–202.
26. Kalofonos H, Rowlinson G, Epenetos AA. Enhancement of monoclonal antibody uptake in human colon tumor xenografts following irradiation. *Cancer Res*. 1990;50:159–163.
27. O'Donoghue JA. The response of tumours with Gompertzian growth characteristics to fractionated radiotherapy. *Int J Radiat Biol*. 1997;72:325–339.
28. Barendswaard EC, Welt S, Divgi CR, et al. Anti-colon cancer monoclonal antibody 100-310 in vitro studies and in vivo localization [abstract]. *Proc Am Assoc Cancer Res*. 1992;33:345.

29. Heath JK, White SJ, Johnstone CN, et al. The human A33 antigen is a transmembrane glycoprotein and a novel member of the immunoglobulin superfamily. *Proc Natl Acad Sci USA.* 1997;94:469–474.
30. Humm JL, Chin LM, Lanza RC, et al. Digital imaging for autoradiography. In: Greene R, Oestmann J, eds. *Computed Digital Radiography in Clinical Practice*. New York, NY: Thieme Medical Publishers; 1991:167–172.
31. Finstad CL, Lloyd KO, Federici MG, et al. Distribution of radiolabeled monoclonal antibody MX35 $F(ab')_2$ in tissue samples by phosphor screen image analysis: evaluation of antibody localization to micrometastatic disease in epithelial ovarian cancer. *Clin Cancer Res*. 1997;3:1433–1442.
32. Barendswaard E, O'Donoghue JA, Larson SM, et al. ^{131}I radioimmunotherapy and fractionated external beam radiotherapy: comparative effectiveness in a human tumor xenograft. *J Nucl Med*. 1999;40:1764–1768.
33. Casarett GW. *Radiation Histopathology.* Vol 1. Boca Raton, FL: CRC Press; 1980.
34. Leichner PK, Klein JL, Siegelmann SS, et al. Dosimetry of I-131-labeled antiferritin in hepatoma: specific activities in the tumor and liver. *Cancer Treat Rep*. 1983;67:647–658.
35. Minsky BD. Management of locally advanced/unresectable rectal cancer. *Radiat Oncol Investig*. 1995;3:97–107.
36. Willett CG, Shellito PC, Tepper JE, et al. Intraoperative electron beam radiation therapy for primary locally advanced rectal and rectosigmoid carcinoma. *J Clin Oncol*. 1991;9:843–849.